Foam is generated in porous media by injecting a water (or CO_2) soluble foaming agent (surfactant) with gas, such as CO_2, either simultaneously (co-injection) or in alternating slugs (SAG). The injection strategy must balance *in-situ* foam generation, propagation, and injectivity constraints. In practice, there are two main injection strategies for *in-situ* CO_2 foam generation [15, 16]. The first is simultaneous injection of CO_2 and surfactant solution known as co-injection. In this case, the quality of the foam is determined by the fraction of gas (f_g) and is a function of flow rate [17]. The second injection strategy is surfactant-alternating gas (SAG), where the surfactant solution and CO_2 are injected in alternating slugs and the quality of the foam depends on the slug sizes of CO_2-to-surfactant solution. At laboratory scale, alternating slugs are not typically used due to small fractional flows of gas and the inability to achieve steady-state [18]. At the field scale, operational constraints influence aspects of the injection strategy. For example, co-injection can be difficult to implement due to extremely low injectivity and associated pressure increases, which minimize throughput [19]. In addition, downhole corrosion can occur from carbonic acid during co-injection of CO_2 and surfactant solution. This has led to a majority of field tests using SAG injection for better injectivity control, especially when operating close to the fracture pressure [20, 21, 22].

Few attempts have been made to characterize unsteady-state *in-situ* CO_2 foam behavior. Therefore, this study attempts to begin establishing a knowledge base for investigating core-scale CO_2 foam injection strategies. The aim is to reduce CO_2 mobility, through the generation of foam, in experiments that are representative of the near wellbore region. This work is part of an ongoing field pilot research program utilizing CO_2 foam for mobility control, EOR, and CO_2 storage in the Permian Basin of West Texas. Miscible CO_2 foam injection will be implemented to reduce high producing gas-oil-ratios, CO_2 recycling, and to provide mobility control for increased CO_2 sweep efficiency. The reservoir pressure in the pilot area is 220 bars, which is close to the formation fracture pressure of 269 bars [23]. An injection strategy must be selected that will not fracture the formation, which would cause problems beyond any remediation by the foam. Thus, the primary objective of this work is to evaluate co-injection and a variety of SAG injection strategies for CO_2 foam mobility control, EOR, and CO_2 storage to assist in the design of the field pilot. A secondary objective is to investigate the impacts of miscibility conditions on *in-situ* foam generation and stability. For more detailed information on the field pilot program see Alcorn et al. (2019).

CO_2 foam was evaluated based upon apparent foam viscosity and its impact on oil recovery. In addition, CO_2 storage potential was measured for each injection strategy. Experimentally, foam behavior by co-injection, single-cycle SAG, and multi-cycle SAG were performed in brine saturated systems to generate foam *in-situ* without the presence of oil. CO_2 foam EOR corefloods were then conducted at first-contact miscible (FCM) and multi-contact miscible (MCM) conditions using *n*-Decane and crude oil, respectively, after waterflooding. A local-equilibrium foam model was fitted from foam stability scans, and experimental results from a CO_2 foam EOR coreflood were used to validate a core-scale numerical model to investigate effects of grid resolution, foam quality, and surfactant. The main objective of the numerical sensitivity study was to validate the foam model in representing the observed foam behavior, which is being extended for use in ongoing field-scale simulations.

2. Materials and Fluids

Outcrop limestone core plugs were used as reservoir analogues due to limited reservoir cores available from the field. Core plugs were drilled with a 2-inch diameter from larger slabs, cut, cleaned and dried before being 100% saturated with synthetic Permian Basin brine under vacuum. Values of porosity and pore volumes were calculated based on weight differential before and after fluid saturation. Absolute permeability was measured by injecting brine until a stable differential pressure was obtained for three different flood rates. Permeability measured for the single core plugs varied between 8mD to 73mD and porosities from 19 to 35%.

Synthetic Permian Basin brine was made based upon water analysis from the field, whereas a light North Sea crude oil was used. The North Sea crude oil has an API of 33.6° (calculated from specific gravity), a little above the API gravity of the Permian Basin crude of 31° at standard conditions. Compositions of brine and crude oil are reported elsewhere [14, 24]. The North Sea crude oil is considered MCM with CO_2 at 60°C and 180 bar, with a minimum miscibility pressure (MMP) of 125 bar [25]. Reservoir conditions for the field test are well above MMP for CO_2 and crude oil. To investigate the effects of miscibility conditions on foam generation and stability a refined oil, *n*-Decane ($C_{10}H_{22}$), was also selected for the first set of EOR corefloods to obtain FCM conditions with CO_2.

A non-ionic surfactant (i.e. Huntsman L24-22) was previously selected for the CO_2 foam field pilot from a surfactant screening study that quantified adsorption on reservoir rock with and without CO_2 present [26]. The non-ionic surfactant was also screened for its ability to alter wettability of oil-wet carbonate rocks to weakly oil-wet conditions in favor of foam generation [14]. The non-ionic surfactant was used at a 1.0 wt% concentration in Permian Basin Brine.

3. Procedure

3.1 Coreflood Set-up

The core-scale system was composed of two stacked core plugs providing a total nominal length of 25 cm to generate foam *in-situ*. Cores with similar porosity and absolute permeability were paired and stacked. An overview of experiments and their stacked system properties are presented in Table 1.

Table 1 – Experimental overview and core properties

ID	Experimental overview	Oil phase	Length [cm]	Porosity [%]	K_{abs} [mD]	S_{wi}
D1	Foam Scan: Co-injection	-	7.5 ± 8.8E-03	24.2 ± 0.2	20.5 ± 0.3	1.00 ± 0.01
D2-D3	Foam Scan: Co-injection	-	12.7 ± 3.5E-03	26.2 ± 0.8	31.6 ± 0.2	1.00 ± 0.01
E2	Foam Stability: SAG	-	12.7 ± 2.0E-03	25.4 ± 0.2	42.3 ± 0.1	1.00 ± 0.01
E3-E4	EOR: Co-injection 1.0 ft/day	n-Decane	24.4 ± 2.8E-03	22.3 ± 1.9	15.5 ± 0.2	0.24 ± 7.22E-03
E5-E6	EOR: Co-injection 2.0 ft/day	n-Decane	24.9 ± 2.8E-03	25.8 ± 0.3	21.4 ± 0.3	0.31 ± 7.28E-03
E7-E8	EOR: Single cycle SAG	n-Decane	27.5 ± 2.8E-03	30.7 ± 2.8	24.0 ± 0.0	0.38 ± 7.59E-03
E9-E10	EOR: Multi-cycle SAG	n-Decane	24.8 ± 2.8E-03	25.1 ± 1.5	38.4 ± 0.4	0.29 ± 7.27E-03
E13-E14	Foam Scan/EOR: Co-injection 1.0 ft/day	Crude oil	24.7 ± 2.8E-03	27.5 ± 0.4	31.4 ± 0.5	0.24 ± 7.13E-03
E15-E16	Foam Scan/EOR: Co-injection 1.0 ft/day (base case[1])	Crude oil	27.4 ± 2.8E-03	22.5 ± 2.3	14.3 ± 1.3	0.15 ± 7.04E-03
E17-E18	EOR: Multi-cycle SAG 1.0 ft/day	Crude oil	24.9 ± 2.8E-03	28.4 ± 1.7	31.6 ± 0.2	0.25 ± 7.20E-03
E21-E22	EOR: Multi-cycle WAG 1.0 ft/day (base case[1])	Crude oil	25.0 ± 2.8E-03	25.8 ± 1.8	21.3 ± 0.7	0.24 ± 7.18E-03

[1]Base case without surfactant solution.
[2]Uncertainty calculated as standard deviation of the mean

The cores were mounted in a horizontally oriented Hassler type core holder and experimental conditions were set to 60°C, to avoid crude oil wax precipitation. Pore pressure was set to 180 bars for CO_2 to be MCM with the North Sea crude oil. At these conditions CO_2 is supercritical and will create an emulsified phase (liquid-in-liquid) with the surfactant solution. A differential pressure transducer and two absolute pressure transducers (i.e. one downstream and one upstream) measured pressure response. The standard setup for high-pressure/high-temperature CO_2 foam injection can be found in [27].

In-situ foam generation, strength, and stability is evaluated by its apparent viscosity, which is quantified from flow rate and pressure drop during foam injection [28]. Foam apparent viscosity is calculated by;

$$\mu_{app} = \frac{k\nabla p}{(u_l + u_g)} \quad (1)$$

where, k is the absolute permeability of the porous media, ∇p is the pressure gradient measured, and u_l and u_g are the superficial velocities of liquid and gas, respectively [17].

3.2 Unsteady-State Foam Stability Scan by SAG

Foam generation and stability was investigated for two modes of SAG injection in a foam stability scan. Single-cycle SAG was run at 100% brine saturated conditions prior to multi-cycle SAG on the same core (E2). A waterflood to re-establish initial conditions with close to zero CO_2 saturation was run in between the foam stability scans. For both SAG injections, pre-determined slug sizes were injected for 4.0 pore volumes (PVs) targeting a gas fraction (f_g) of 0.70. For single-cycle SAG, a single slug of surfactant solution was injected (1 PV) before CO_2 was introduced for 3 PVs. For multi-cycle SAG, 12 rapid cycles were run: each cycle consisting of a surfactant slug of 0.11 PVs and a CO_2 slug of 0.22 PVs. Un-steady state apparent foam viscosities were calculated as a function of time (i.e. PVs injected) using Equation 1.

3.3 Steady-State Foam Quality and Rate Scans by Co-injection

Foam generation and stability during co-injection was assessed by foam quality and rate scans. Tests were run in 100% brine saturated cores, where one system was composed of a single core (D1) and the other a stacked system (D2-D3). Scans were also performed at residual oil saturation after CO_2 foam EOR to investigate the effect of residual oil on foam stability (E13-E14), and equivalently for a base case without surfactant (E15-E16). See Table 1 for experimental overview.

Foam quality scans determine the optimal gas fraction (f_g) that will generate the highest apparent viscosity during co-injection. CO_2 fractions were changed from 0.0 to 0.90 for drainage-like co-injection (i.e. increasing CO_2 fraction) at a total superficial injection rate of 1.0 ft/day. Each fraction was injected until steady state pressure drop was achieved before increasing to the next fraction. The apparent foam viscosity was calculated from Equation 1. Rate scans were performed following foam quality scans on the same core(s) to estimate rate-dependency on shear-thinning behavior. Rate scans for co-injection were run by increasing the total injection rate at the optimal CO_2 fraction from quality scans. Starting at a superficial velocity of 1.0 ft/day, the injection rate was increased to 2.0, 3.0, and 4.0 ft/day after reaching steady-state conditions.

3.4 CO_2 Foam EOR

Core plugs were initially 100% brine saturated, stacked, and drained with either *n*-Decane or dead crude oil to irreducible water saturation (S_{wi}) at a constant pressure drop of 2 bar/cm. A waterflood was performed for 1 PV prior to CO_2 foam injection. Injection strategies during CO_2 foam were either co-injection, single-cycle, or multi-cycle SAG. CO_2 foam was injected for no more than 2 PVs, considering volumetric and economic limitations at the field-scale. Produced fluids were measured at ambient conditions as stock tank volumes. Density and compressibility were considered negligible for the specific dead crude oil and refined oil used in these experiments. Saturations were calculated based upon the difference in initial oil in place and oil produced divided the total pore volume.

CO_2 foam EOR was performed at FCM conditions using *n*-Decane and at MCM conditions using North Sea crude oil. At FCM conditions, CO_2 foam co-injection used two injection rates (1.0 ft/day for E3-E4 and 2.0 ft/day for E5-E6) to investigate the shear-thinning behavior of foam

during EOR. Co-injection results were then compared with single cycle (E7-E8) and multi cycle SAG (E9-E10). The most promising (highest apparent foam viscosity and oil recovery) injection strategies were evaluated at MCM conditions, with crude oil, and compared with base case experiments without surfactant solution.

3.5 Core-Scale Model Set-up

Laboratory data from a co-injection experiment (E13-E14) was utilized for a core-scale simulation model. The model was initialized to represent the stacked system during waterflood and co-injection. For the waterflood, simulations were conducted with ECLIPSE 100 Blackoil simulator while the compositional simulator E300 (Schlumberger, 2015.2) was used for co-injection. Experimental data validated the model through matching bottom hole pressure (BHP) and cumulative oil/water production. The validated model was used to conduct a sensitivity analysis on the effect of grid cell size, foam quality, and surfactant on oil recovery and CO_2 mobility reduction. The main objective was to ensure model robustness at representing the observed foam behavior, which is extended to use in ongoing field scale simulations.

The base case model consisted of a rectangular grid with dimensions 1 x 1 x 100 (x, y, z). The length of the model was identical to the experimental core system length of 24.7 cm. The model and individual grid cells were also consistent with the core diameter of 4.8 cm thus, each individual grid cell measured 4.8 x 4.8 cm in the x- and y-directions. The injector was located in the first grid block (inlet), while the producer was located in the last grid block (outlet). The production well was placed on BHP control and the injector was controlled by rate both of which were measured in the laboratory. Relative permeability data for the waterflood was derived from JBN analysis of oil and water displacement during the laboratory experiment [29]. Oil and water densities and viscosities were available from PVT-analysis of the crude oil. The model was initiated with S_{wi} of 0.24 at a system pressure of 182 bars.

The co-injection was initialized at pressure and saturations from the history-matched waterflood. The grid size, orientation, well completions and controls were kept identical, except two injection wells were used to represent the single co-injection well from the experiment (one for CO_2 and one for surfactant solution). A compositional simulation case was generated which contained 14 oil components and 2 water components (water and surfactant). Relative permeability curves were derived from CO_2/brine displacement experiments on similar core material described elsewhere [23]. Despite their influence on foam behavior, capillary pressure effects were not included in this study. This is an area, which merits further investigation.

The injection schedule was identical to the experimental procedure and a foam quality of 70% was targeted using a surfactant solution concentration of 1.0 wt%. The effect of foam was modeled using an empirical local-equilibrium approach where the gas relative permeability in the presence of foam is modified by multiplying the gas relative permeability without foam by a mobility reduction factor (MRF) [30]. The mobility reduction factor is dependent upon water saturation, oil saturation, surfactant concentration and shear rate. A maximum gas mobility reduction (*fmmob*) is also used to set the maximum mobility reduction that can be achieved by foam. These parameters were derived from foam quality and rate scans and fit to the empirical model by curve fitting regression [23, 30].

4. Results and Discussion

Apparent viscosities and incremental oil recoveries were used to evaluate foam generation, stability, and EOR performance during CO_2 foam injection. Several mechanisms contribute to the foam apparent viscosity (and pressure response) including foam generation, trapped gas, and CO_2-surfactant emulsification.

4.1 Unsteady-State Foam Stability by SAG

CO_2 foam stability scans by single-cycle and multi-cycle SAG injections were compared in initially brine saturated systems without oil present (Figure 1). Foam apparent viscosity during single-cycle SAG was 18.2 ± 2.7 cP (dashed curve, Figure 1), and 120.2 ± 0.3 cP for multi-cycle SAG (solid curve, Figure 1). Based upon the increase in apparent viscosity, foam was generated when the first CO_2 slug was injected for both injection modes (Figure 1).

During single-cycle SAG, foam generation occurred within the first PV of CO_2 injected and foam remained stable for the next 2 PV with only a slight dry-out effect towards the end of injection (black dashed curve, Figure 1). Injecting multiple alternating slugs of surfactant solution and CO_2 improved conditions for foam generation and stability. During multi-cycle SAG, surfactant solution was introduced to the system in an imbibition process, which caused a decrease in capillary pressure, likely triggering foam generation. This change in capillary pressure is advantageous for foam generation since the creation of lamella requires exceeding a minimum pressure gradient. Hence, a decrease in capillary pressure during the surfactant slugs improved conditions for foam generation. Increased wetting-phase saturation during surfactant solution slugs also may have mitigated foam dry-out. The growth and propagation of a stable high apparent viscosity foam was clear during multi-cycle SAG (solid curve, Figure 1).

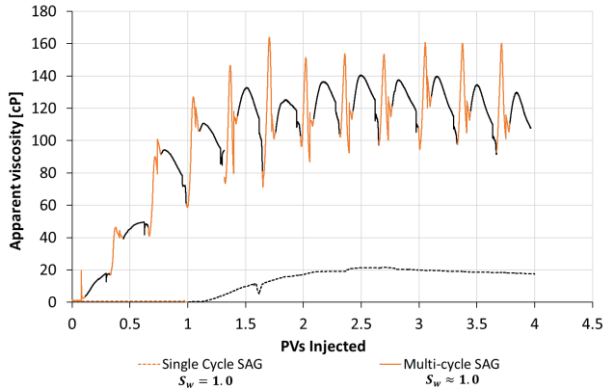

Fig. 1. Foam apparent viscosity as a function of pore volumes injected during single-cycle SAG (dashed curve) and multi-cycle SAG (solid curve). Orange curves represent surfactant solution slugs and the black curves are CO_2 slugs. Single cycle SAG was initiated at $S_w = 1.0$ (no trapped CO_2), whereas multi-cycle SAG injection was initiated with a nominal amount of trapped CO_2 in the core, $S_w \approx 1.0$.

The first CO_2 injection during multi-cycle SAG (from 0.11 to 0.33 PV) is equal to the first CO_2 injection of the single-cycle SAG (from 1 to 1.22 PV), except the amount of surfactant injected (which should benefit single-cycle). We can therefore directly compare the first cycle of the experiments, and evidently, the foam generation is much more immediate and rapid in the multi-cycle experiment, resulting in 15 cP increase in apparent viscosity when 0.22 PV is injected, compared with < 5 cP during the single-cycle. It took 5 cycles to reach peak foam strength of 120 cP during the multi-cycle SAG, where each step had an average increase in apparent viscosity of 25 cP. Extrapolating the observed behavior of the first 0.22 PV of the single-cycle experiment for five consecutive cycles to reach peak apparent viscosity, would result in final apparent viscosity of 25 cP.

Despite efforts to return the core to 100% water saturation, the presence of trapped CO_2 from the previous single-cycle SAG experiment likely reduced CO_2 relative permeability and increased the pressure drop during multi-cycle SAG. This would result in higher foam apparent viscosities. A decrease in effective water permeability was observed for E2 from 42.3 mD to 19.8 mD by capillary trapped CO_2 prior to multi-cycle SAG foam stability. However, during multi-cycle SAG, the step-wise increase in differential pressure and significantly increased apparent viscosity compared to single-cycle SAG suggest that the alternating injection scheme did improve conditions for foam generation and stability.

4.2 Steady-State Foam Quality and Rate Scans by Co-injection

Figure 2 shows co-injection foam quality scans, D1 and D2-D3 (orange and green curves), which have previously been published [14, 31] and are shown here for comparison.

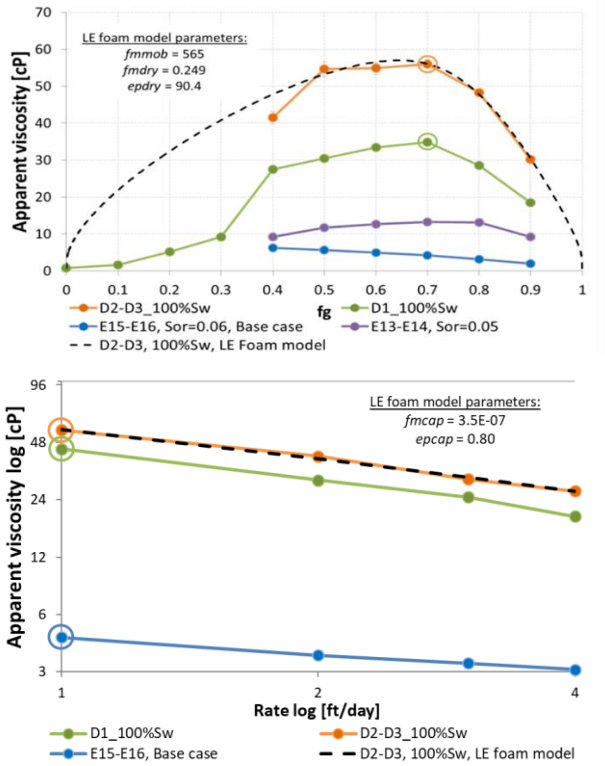

Fig. 2. Foam quality scans f_g = 0.0 to 0.90 (top) and foam rate scans at 1.0, 2.0, 3.0 and 4.0 ft/day (bottom) during co-injection of CO_2 and surfactant solution. Foam model parameters derived from the experiments are also shown.

Peak apparent foam viscosities at steady state for f_g = 0.70 was 34.9 ± 1.0 cP (D1), and 56.0 ± 1.6 cP (D2-D3), higher than single-cycle SAG (18.2 ± 2.7 cP), but lower than multi-cycle SAG (120.2 ± 0.3 cP) in Figure 1. The foam strengths measured during the two co-injections are relatively similar, considering the heterogeneous core, but discrepancy remains when comparing the three co-injection experiments to the SAGs. It is likely that the injection scheme is not the only explanation for the variation in apparent viscosities.

Foam quality scans with residual oil also investigated the influence of crude oil on foam stability. Experiment E13-E14 in Figure 2 (purple curve) was performed after CO_2 foam EOR at a residual oil saturation (S_{or}) = 0.05 (purple curve, Figure 2). A lower apparent foam viscosity was observed for every f_g compared to foam quality scans conducted with 100% initial water saturation (i.e. strongly water-wet) in Figure 2 (orange and green curves). However, apparent viscosities at fg = 0.70 were 13.20 cP for experiment E13-E14 with surfactant (purple curve, Figure 2) compared to 4.19 cP for the base case (E15-E16, blue curve, Figure 2) at S_{or} = 0.06, without surfactant. Hence, these experiments show that this foam system is capable of generating foam with low apparent viscosities when crude oil is present.

4.3 CO_2 Foam EOR

4.3.1 First-Contact Miscible Conditions

Co-injection and SAG injection strategies were evaluated based upon their apparent viscosity and oil recovery at

FCM conditions (Figure 3). The initial waterfloods recovered between 31.2 % and 47.7% OOIP and a clean water cut was observed for all experiments (left of the vertical black dashed line). The range in waterflood recovery can be attributed to core heterogeneity [32]. Recovery factors and apparent viscosity values are listed in Table 2.

CO_2 foam co-injections were performed at two different injection rates (1.0 ft/day and 2.0 ft/day) to investigate shear-thinning behavior during EOR corefloods (Figure 3). Foam was generated earlier at higher rate (at 1.7 PVs injected, E5-E6, orange dashed curve) compared to the lower co-injection rate (at 2.3 PVs injected, E3-E4, orange solid curve) from dynamic observations of apparent viscosity. The average apparent viscosity, however, was higher at 1.0 ft/day (28.1 cP, E3-E4) than for 2.0 ft/day (18 cP, E5-E6) for the last 0.5 PVs injected (Table 2). This is an indication of the shear-thinning behavior of foam at increasing flow rates. Shear-thinning behavior was also observed in foam rate scans shown in Figure 2 (bottom).

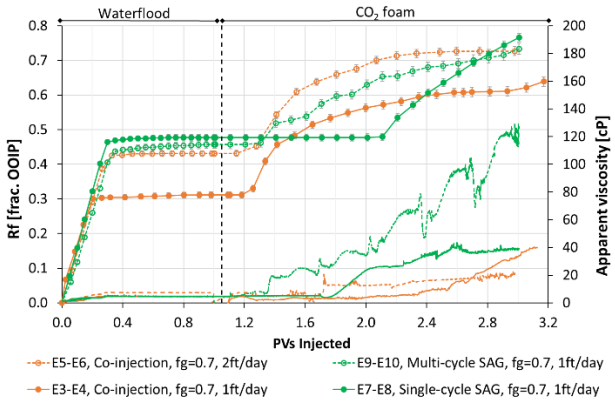

Fig. 3. Recovery factor vs. PVs injected for CO_2 foam EOR corefloods with co-injection and SAG under FCM conditions with *n*-Decane. The orange curves represent CO_2 foam by co-injection at rates of 1.0 ft/day (closed circles) and 2.0 ft/day (open circles), and the green curves are single-cycle SAG (closed circles) and multi-cycle SAG (open circles). The vertical dashed black line separates the waterflood to the left from the CO_2 foam flood to the right. The secondary y-axis shows apparent viscosity.

Table 2. Recovery factors for CO_2 foam EOR corefloods

Core ID	Injection Strategy	Oil phase	$R_{f,\,WF}$ [%OOIP]	$R_{f,\,CO2\,foam}$ [%OOIP]	$R_{f,\,tot}$ [%OOIP]	Apparent visc. CO_2 foam [cP][1]	S_o (after WF)
E3-E4	Co-injection	n-Decane	31.2 ± 0.9	32.7 ± 1.7	63.9 ± 1.4	28.1 ± 7.7	0.48
E5-E6	Co-injection	n-Decane	43.1 ± 0.8	29.6 ± 1.5	72.7 ± 1.2	18.0 ± 1.4	0.39
E7-E8	Single-cycle SAG	n-Decane	47.7 ± 0.8	28.9 ± 1.5	76.6 ± 1.2	37.9 ± 1.1	0.48
E9-E10	Multi-cycle SAG	n-Decane	45.7 ± 1.1	27.6 ± 1.9	73.3 ± 1.6	100.7 ± 14.6	0.46
E13-E14	Co-injection	Crude oil	62.0 ± 0.9	31.0 ± 1.6	93.0 ± 1.3	5.5 ± 0.5	0.29
E15-E16	Co-injection[2]	Crude oil	58.6 ± 1.0	34.9 ± 1.7	93.5 ± 1.4	7.3 ± 0.1	0.35
E17-E18	Multi-cycle SAG	Crude oil	62.3 ± 0.9	30.5 ± 1.6	92.8 ± 1.3	7.0 ± 3.0	0.28
E21-E22	Multi-cycle WAG[2]	Crude oil	66.8 ± 1.0	33.2 ± 1.8	100.0 ± 1.4	7.3 ± 1.6	0.25

$R_{f,WF}$ = recovery factor by waterflood; $R_{f,\,CO2foam}$ = recovery factor by CO_2 foam; $R_{f,tot}$ = total recovery factor
[1]Mean average last 0.5PVs at the end of the CO_2 foam flood. Uncertainties are given as standard deviation of the mean.
[2]Base case without surfactant.

Apparent viscosity trends during SAG EOR (green curves, Figure 3) were the same as for foam stability scans without oil present (Figure 1). The increase in apparent viscosity was more rapid for each SAG injection (green curves) than either of the co-injection experiments (orange curves), likely due a faster increase in CO_2 saturation. However, it is possible that a higher apparent viscosity could have been obtained by continuing the co-injection at 1.0 ft/day (Figure 3, solid orange curve). CO_2 foam apparent viscosity for multi-cycle SAG (Figure 3, dashed green curve) increased continuously for each cycle and reached an average value of 100.7 cP at the end of injection. In terms of mobility control, multi-cycle SAG was superior in creating conditions for high viscous displacement during EOR corefloods at FCM conditions (Figure 3).

The presence of the alkane *n*-Decane oil did not negatively influence foam generation or propagation for either injection strategy (Figure 3). *N*-Decane is a non-polar oil molecule with has no ability to alter wetting-state like that of heavy polar molecules (i.e. asphaltenes and resins). Aging carbonate rock in *n*-Decane does not alter wettability [33] and so stable foam was able to be created *in-situ*, even in the presence of oil.

Accelerated oil recovery rate was observed from the start of both co-injections (Figure 3, open and closed orange circles) and most of the oil was produced after 1.0 PV of CO_2 foam injected. For single-cycle and multi-cycle SAG (solid green circles), no oil was recovered during the initial surfactant slug before CO_2 was injected. Thus, diffusion dominated oil recovery above that of viscous displacement by foam at FCM conditions. CO_2 diffusion is a dominant recovery mechanism at core-scale with the potential to recover nearly 100% of the oil [34, 35]. At constant f_g = 0.70, CO_2 diffusion recovered the same amount of oil regardless of injection mode, on average 29.7 ± 2.2% OOIP. As observed in Figure 3, however, total recoveries did not reach the ultimate recovery potential of 100% OOIP. This is because stable foam lamellas can create barriers that hinder direct contact between the discontinuous CO_2 phase and unrecovered oil, negatively impacting oil recovery. Values of incremental oil recovery during CO_2 foam are listed in Table 2.

4.3.2 Multiple-Contact Miscible Conditions

Viscous forces are desirable for mobility control and fluid diversion during CO_2 foam EOR. Co-injection at 1.0 ft/day and multi-cycle SAG gave best results in terms of both apparent viscosity and EOR at FCM conditions. These injection strategies were therefore used to determine sensitivity in presence of multicomponent crude oil at MCM conditions. Base case experiments were also performed without surfactant solution as a reference. Results are presented in Figure 4.

The initial waterflood recovered on average 62.0 ± 2.8% OOIP (blue curves, Figure 4) with two-phase production, a characteristic of less water-wet conditions [36]. The measured apparent viscosities during CO_2 foam experiments demonstrated little to no *in-situ* foam generation. No increase in foam apparent viscosity was observed above that of the base cases without surfactant. Two possible explanations are offered for the absence foam generation:

- Oil composition is known to influence lamella creation and foam stability, and its presence can make some foams more unstable than others. Foam stability can be reduced with decreasing carbon content in crude oils. It has also been observed elsewhere that a lower number alkanes are more destabilizing than higher number alkanes, because their shorter hydrocarbon chains are more easily imbibed into foam plateau borders to solubilize with surfactants leading to oil spreading and foam instability [10, 37-39].

- Wettability alteration by crude oil towards less water-wet conditions can hinder foam generation and strength. It has previously been reported that foam cannot be generated at wettability conditions other than strongly water-wet due to the lack of water-wet snap-off sites [40, 16, 13]. The multi-component crude oil likely induced a shift towards oil-wet conditions, which caused the lamellas to detach from the pore walls, restricting foam generation.

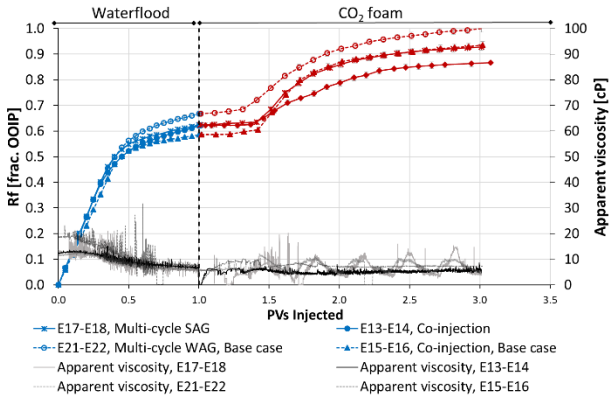

Fig. 4. Recovery factor vs. PVs injected for EOR corefloods by co-injection and multi-cycle SAG under MCM conditions. Left of the vertical dashed black line is waterflood (blue curves) and to the right is CO_2 foam (red curves). CO_2 foam injections are represented by the solid lined curves, while the base cases are dashed lines. The secondary y-axis shows apparent viscosity.

CO_2 foam oil recoveries were on average 30.6 ± 3.0% OOIP for all injection strategies with and without surfactant, at both FCM and MCM conditions. Therefore, incremental oil recoveries were also driven by CO_2 diffusion at MCM conditions (Figure 4). Bernard and Holm observed the same effect in their core-flood experiments with CO_2 foam [44]. This restricts evaluation of injection strategies in terms of production efficiency. Longer induction periods were observed, however, for continuous oil banks to develop under MCM conditions in Figure 4. Between 0.3 to 0.4 PVs of CO_2 foam were injected before oil production was observed (red curves). Total recoveries were higher at MCM conditions (93.2 ± 2.7% OOIP) compared to FCM conditions (71.2 ± 3.2% OOIP) as the waterfloods at MCM conditions left behind lower residual oil saturations (Table 2). Further sensitivity analysis on the effect of CO_2 fractions on foam behavior was considered using the history-matched core-scale simulation model.

4.4 Associated CO_2 Storage

A secondary objective for implementing CO_2 foam for mobility control in EOR is the potential for storing CO_2 as a part of carbon capture, utilization, and storage (CCUS). To calculate CO_2 stored, the volume of CO_2 produced was measured from volumetric conservation of injected and produced fluids, and subtracted from the volume of CO_2 injected. Calculations were made for the FCM and MCM experiments. Based upon mass balance, the value for CO_2 storage (given as a fraction of total PV) is equal to the saturation change of oil and water in the core after CO_2 foam.

Figure 5 shows CO_2 storage in fraction of PV for both co-injections (top) and multi-cycle SAGs (bottom). A direct correlation between the amounts of CO_2 stored and the water/oil saturation change was observed regardless of injection strategy. For every amount of fluid produced, the equivalent amount of CO_2 was stored. CO_2 storage potential was 9.0% greater for multi-cycle SAGs compared to co-injections at MCM. However, CO_2 storage potential was 17.1% greater at FCM conditions (for either injection strategy), compared to MCM, due to improved CO_2 foam displacement and increased CO_2 trapping by capillary forces in more water-wet core plugs.

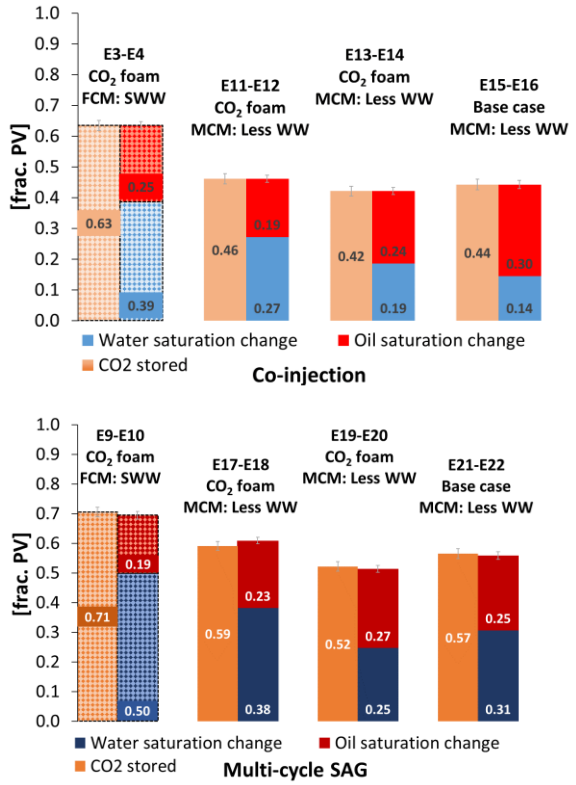

Fig. 5. CO_2 storage potential during CO_2 foam EOR corefloods at FMC and MCM conditions. Top: Co-injection CO_2 foam floods and base case (without surfactant). Bottom: Multi-cycle SAG CO_2 foam floods and base case. Orange bars represent CO_2 stored in fraction of total PV, and the blue and red bars are fractional change in water and oil saturation, respectively. Textured bars indicate FCM conditions, whereas solid bars are experiments at MCM conditions. Note wettability of cores at top of each bar.

4.5 Core-Scale Model Validation and Sensitivity Study

The core-scale simulation model utilized the foam stability measurements in Figure 2 to fit the empirical local equilibrium foam model by curve fitting regression [23, 30]. The value for the maximum gas mobility reduction, *fmmob*, however, was reduced to 41.5 in agreement with previous findings on field core material to reflect more realistic conditions for the field system. An acceptable history-match for experiment E13-E14 was obtained for both waterflood and co-injection. The waterflood match was achieved by tuning the oil relative permeability curve to match oil/water production rate and BHP. The co-injection was matched by tuning the oil and water relative permeabilities to match cumulative oil/water production and BHP. Figure 6 shows the history-match.

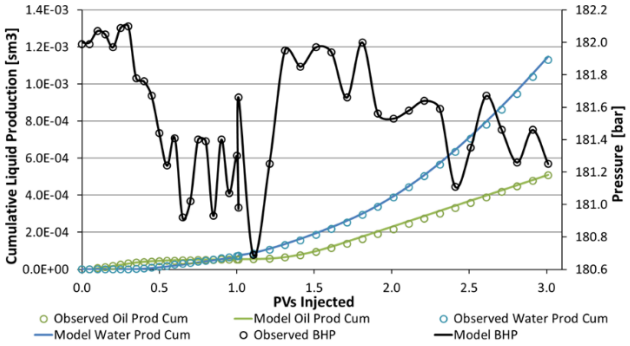

Fig. 6. Observed (open circles) and modeled (curves) cumulative oil/water production during waterflood and co-injection of the history-matched experiment. Production well BHP is shown on the secondary y-axis.

The validated model was first used to investigate the effect of grid resolution during co-injection. The generated case was identical to the base case history-match, but used the fine scale grid (5 times finer in the x, y, and z directions) to evaluate change in CO_2 mobility reduction and oil recovery. CO_2 mobility reduction is generally inferred from delayed CO_2 breakthrough and an increased response in injection pressure. However, simulation results showed limited effect of grid resolution on co-injection in terms of injection well pressures, CO_2 breakthrough, and cumulative recoveries. As limited variations were observed, with the fine grid model, further sensitivity studies utilized the coarser base grid.

4.5.1 Effect of Foam Quality

The effect of foam quality (CO_2 fraction) was studied using the base grid to determine its impacts on oil recovery and CO_2 mobility reduction. Cases injecting higher CO_2 fractions were set to assess model sensitivity on amounts of CO_2 injected and its influence on oil recovery. The base case history-matched model used the optimal CO_2 fraction of 0.70 measured in laboratory. Further sensitivity cases were set to CO_2 fractions of 0.80, 0.90, and 0.95. Figure 7 shows cumulative oil production (solid curves) for the base case (f_g=0.70) and CO_2 fraction sensitives. With increasing CO_2 fractions, the oil recovery rate accelerated but all cases recovered the same volume of cumulative oil. Hence, CO_2 miscibility dominated oil displacement as also observed in the CO_2 foam EOR corefloods experiments in Figure 3 and 4.

Injection pressures for the various CO_2 fractions are shown in Figure 7 (dashed curves). All injection pressures followed the same trend. Higher pressures, however, were observed as the fraction of CO_2 decreased and the fraction of surfactant solution increased, creating a higher apparent viscosity foam (blue and red dashed curves, Figure 7). This is consistent with trends observed in foam quality scans where the optimal CO_2 fraction and highest apparent viscosity was observed at 0.70 (cf. Figure 2, left, green and orange circles). At fractions above this, apparent viscosities declined.

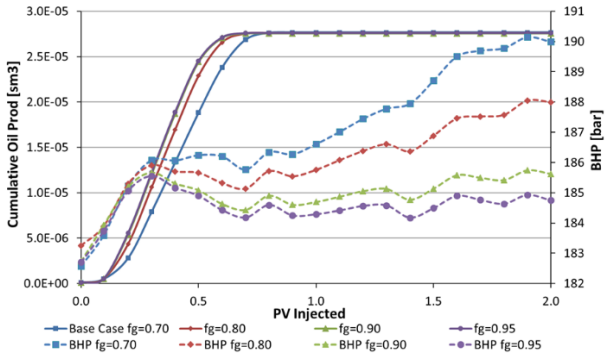

Fig. 7. Cumulative oil production versus time for the base case (blue solid curve), and three sensitivities with different gas (CO_2) fractions. Injection pressure versus time shown on the secondary y-axis for the base case (blue dashed curve), and three sensitivities with different gas (CO_2) fractions.

4.5.2 Effect of Surfactant

CO_2 diffusion and miscibility are evidently the dominant oil recovery mechanisms in both simulation and laboratory experiments. Therefore, a similar case to the history-matched experiment was set-up without surfactant to investigate pure CO_2 versus CO_2 foam displacement. The injection schedule was kept identical to the base case co-injection, except only water was injected as the aqueous phase. Figure 8 shows injection pressure (dashed curves) and cumulative CO_2 production (solid curves) during co-injection with surfactant (blue curves) and without surfactant (red curves).

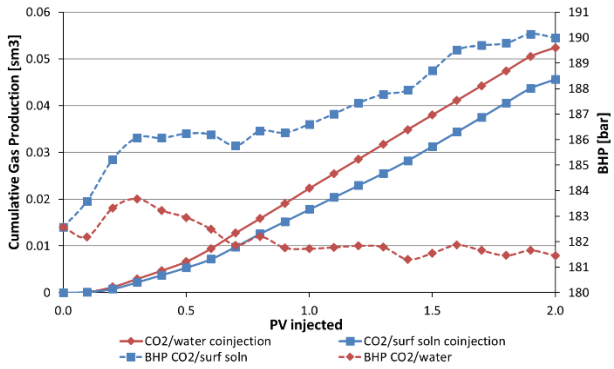

Fig. 8. Injection well pressure (dashed curves) and cumulative gas (CO_2) production (solid curves) for the base case with surfactant present (blue curve) and a case without surfactant present (red curves).

The injection well pressure was significantly lower for the case without surfactant compared to the base case with surfactant (Figure 8, red dashed curve). This indicated higher CO_2 mobility and increased CO_2 production in absence of foam (Figure 8, red solid curve). Analysis of liquid production showed the same cumulative volume of oil recovered in both cases (green curves, Figure 9), but additional water was produced during CO_2 foam injection (blue dashed curve). Hence, a larger storage potential for CO_2 was obtained with CO_2 foam displacement. Similar behavior was also observed in Figure 5, where CO_2 storage was higher for multi-cycle SAG because of increased water displacement during foam injection compared to CO_2 alone.

The similar volumes of oil produced with and without surfactant, demonstrated the dominance of CO_2 miscibility over viscous displacement by foam (green curves, Figure 9). The core-scale model is consistent with laboratory observations indicating that miscibility and diffusion are the governing displacement forces in small core-scale systems. This creates a challenge when upscaling core-scale foam behavior to the field-scale as reservoir heterogeneity and gravity effects will likely be more dominant in the field.

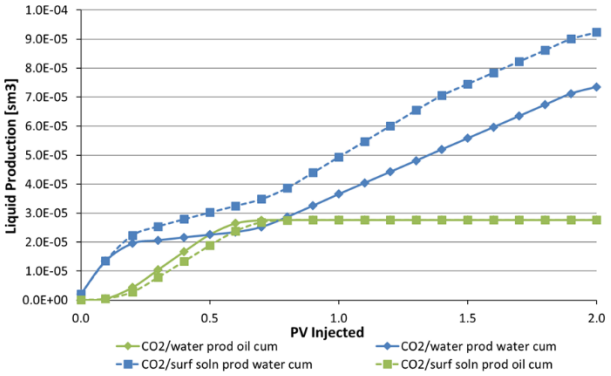

Fig. 9. Cumulative liquid production during CO_2/water co-injection (solid curves) and CO_2/surfactant solution (dashed curves). Green curves correspond to cumulative oil produced and blue to cumulative water.

5. Conclusions

This work investigated various injections strategies (co-injection and SAG) for CO_2 foam mobility control, EOR and CO_2 storage to assist in the design of a CO_2 foam field pilot. The sensitivity study involved both experimental laboratory work and numerical modeling. Supercritical CO_2 foam behavior in brine-saturated systems was investigated to generate foam *in-situ*, without the presence of oil. Additionally, CO_2 foam EOR corefloods were conducted in the presence of refined oil at first-contact miscible (FCM) conditions and in the presence of crude oil at multiple-contact miscible (MCM) conditions after waterflooding to investigate the impact of oil and miscibility on foam generation and stability. Key findings from this work are:

- Multi-cycle SAG resulted in the highest apparent viscosity foam of 120.2 cP during *in-situ* CO_2 foam stability scans compared to co-injection (56.0 cP) and single-cycle SAG (18.2 cP) without oil present. Multi-cycle SAG also achieved the highest apparent viscosity foam of 100.7 cP for the CO_2 foam EOR corefloods, with refined oil present, at FCM conditions.
- Incremental oil recoveries during tertiary CO_2 foam injections were on average 30.6% OOIP for all injection strategies, with and without surfactant, at both FCM and MCM conditions. At MCM conditions, CO_2 foam was not generated as a result of wettability

alteration by crude oil and foam destabilization in presence of crude oil.

- CO_2 diffusion and miscibility with oil were the dominant recovery mechanisms as observed in laboratory corefloods and numerical core-scale sensitivity studies on foam quality.
- A validated numerical core-scale model captured the observed foam behavior from laboratory corefloods. The foam model was not sensitive to grid resolution and corroborated laboratory observations of core-scale foam behavior. Further work is ongoing to upscale the laboratory observations to field-scale simulations.
- A direct correlation between the amounts of CO_2 stored and water/oil saturation change was observed in the laboratory corefloods. For every amount of fluid produced, the equivalent amount of CO_2 was stored regardless of injection strategy. CO_2 storage potential was 17.1% greater at FCM conditions, compared to MCM, due to increased displacement by CO_2 foam and CO_2 trapping by capillary forces in more water-wet core plugs. Core-scale simulations indicated higher CO_2 storage potential with CO_2 foam because of increased water displacement, compared to cases without foam.

Reservoir heterogeneity and gravity dominate displacement at the field-scale, therefore the high apparent viscosities and viscous displacement forces provided by multi-cycle SAG in the foam stability scans are favorable. The shear-thinning behavior of the foam system can also mitigate injectivity loss near the injection well, where flow rates are high. Additionally, a SAG injection scheme provides better injectivity control, when operating close to formation fracture pressure, due to the ability to switch to CO_2 injection for foam dry-out. Reported oil recoveries, from CO_2 foam EOR corefloods, cannot be upscaled to predict field performance as CO_2 diffusion will have less effect on displacement at the length scales existing in the field.

Acknowledgements

The authors wish to acknowledge the Norwegian Research Council CLIMIT program for financial support under grant number 249742 - *CO_2 Storage from Lab to On-Shore Field Pilots Using CO_2-Foam for Mobility Control in CCUS* and industry partners; Shell Global Solutions, TOTAL E&P USA, Inc., and Equinor ASA. The authors also thank the field operator for cooperation.

Nomenclature

API	American Petroleum Institute
BHP	bottom hole pressure
CCUS	carbon capture, utilization, and storage
EOR	enhanced oil recovery
FCM	first-contact miscible
f_g	gas fraction
fmmob	maximum gas mobility reduction
K	permeability
MCM	multiple-contact miscible
MMP	minimum miscibility pressure
MRF	mobility reduction factor (foam model)
OOIP	oil originally in place
PV	pore volume
PVT	pressure, volume, temperature
$R_{f,tot}$	total recovery factor
$R_{f,WF}$	recovery factor by waterflood
$R_{f,\ CO2\ foam}$	recovery factor by CO_2 foam
SAG	surfactant-alternating-gas
S_{wi}	irreducible water saturation
S_o	oil saturation
S_{or}	residual oil saturation
t	time
u_g	gas superficial velocity
u_{liq}	liquid superficial velocity
μ_{app}	apparent viscosity
∇p	pressure gradient
SWW	strongly water-wet
WW	water-wet

References

1. Bernard, G.G., Holm, L.W. and Harvey, C.P. (1980). Use of Surfactant to Reduce CO_2 Mobility in Oil Displacement. *SPE Journal* **20** (4): 281-292.
2. Latil, M. *Enhanced Oil Recovery* (1980) Paris: Editions Technip.
3. Bond, D.C. and Holbrook, O.C. Gas Drive Oil Recovery Process. (1958) United States Patent Office. 30 December. Patented number 2,866,507.
4. Nzekwu, B.I. and Bennion, D.W. (1987) Mobility Control in Dynamic Gravity Segregation Flow Systems. *Journal of Canadian Petroleum Technology* **26** (4): 80-87. JCPT87-04-08.
5. Rossen, W.R. (1996). Foams in Enhanced Oil Recovery. In Foams Theory, Measurements, and Applications. eds. Prud'homme, R.K. and Khan, S.A. **57**, ch. 11, 414-464, Marcel Dekker, Inc. New York
6. A.H. Falls, G.J. Hirasaki, T.W. Patzek, P.A. Gauglitz, D.D. Miller, and T. Ratulowski. (1988). *SPE Reserv Eng*. **3**: 844
7. Holm, L.W. (1968). The Mechanisms of Gas and Liquid Flow Through Porous Media in the Presence of Foam. *Transactions* **243**, 359-369.
8. Bernard, G.G., Holm, L.W. and Jacobs, W.L. (1965). Effect of Foam on Trapped Gas Saturation and on Permeability of Porous Media to Water. SPE Annual Fall Meeting, 3-6 October, Denver, Colorado, US. SPE-1204.
9. Emadi, A., Sohrabi, M., Farzaneh, S.A. and Ireland, S. (2013). Experimental Investigation of Liquid-CO2 and CO2-Emulsion Application for Enhanced Heavy Oil Recovery. SPE EAGE and SPE Europec, 10-13 June, London, United Kingdom. SPE-164798-MS.
10. Schramm, L.L. and Novosad. (1992). The destabilization of foams for improved oil recovery by crude oils: Effect of the nature of the oil. *Journal of Petroleum Science and Engineering* **7** (1-2), 77-90.
11. Prud'homme, R K. and Khan, S A. (1996). Foams, Theory, Measurements, and Applications. New York: Marcel Dekker Incorporated.
12. Farajzadeh, R., Andrianov, A., Krastev, R., Hirasaki, G.J. and Rossen, W.R. (2012). Foam-oil interactions

in porous media: Implications for foam assisted enhanced oil recovery. Advances in Colloid and Interface Science 183-184, 1-13.

13. Schramm, L.L. and Mannhardt, K. (1996). The effect of wettability on foam sensitivity to crude oil in porous media". *Journal of Petroleum and Engineering* **15** (1), 101-113.
14. Fredriksen, S., Alcorn, Z., Frøland, A. et al. (2019). Surfactant Prefloods During Carbon Dioxide Foam Injection for Integrated Enhanced Oil Recovery in Fractured Oil-Wet Carbonates. *SPE Journal*. SPE-190168-PA (in press; posted 5 April 2019). https://doi.org/10.2118/190168-PA.
15. Shan, D. and Rossen, W.R. (2002). Optimal Injection Strategies for Foam IOR. SPE/DOE Improved Oil Recovery Symposium, 13-17 April, Tulsa, Oklahoma. SPE-75180-MS.
16. Farajzadeh, R., Andrianov, A., Krastev, R., Hirasaki, G.J. and Rossen, W.R. (2012). Foam-oil interactions in porous media: Implications for foam assisted enhanced oil recovery. *Advances in Colloid and Interface Science* **183-184**, 1-13.
17. Jones, S.A., Laskaris, G., Vincent-Bonnieu, S., Farajzadeh, R. and Rossen, W.R. (2016). Surfactant Effect on Foam: From Core Flood Experiments To Implicit-Texture Foam Model Parameters. SPE Improved Oil Recovery Conference, 11-13 April, Tulsa, Oklahoma. SPE-179637-MS.
18. Groenenboom, J., Kechut, N.I., Mar-Or, A., Vincent-Bonnieu, S. (2017). Foam Assisted WAG: Injection Strategies to Optimize Performance. SPE/IATMI Asia Pacific Oil & Gas Exhibition, 17-19 October, Jakarta, Indonesia. SPE-186991-MS.
19. Hoefner, M.L. and Evans, E.M. (1995). CO_2 Foam: Results from Four Developmental Fields Trials. *SPE Reservoir Engineering* **10** (4), 273-281.
20. Chou, S.I., Vasicek, S.L., Pisio, D.L., Jasek, D.E., Goodgame, J.A. (1992). CO2 Foam Field Trial at North Ward Estes. 67th SPE Annual Technical Conference and Exhibition, October 4-7, Washington, D.C.
21. Harpole, K.J., Siemers, W.T. and Gerard, M.G. (1994). CO_2 Foam Field Verification Test at EVGSAU: Phase IIIC – Reservoir Characterization and Response to Foam Injection. SPE/DOE 9th Symposium on Improved Oil Recovery, 17-20 April, Tulsa, OK, USA.
22. Henry, R.L.; Fisher, D.R.; Pennel, S. P.; Honnert, M.A. (1996). Field Test of Foam to Reduce CO2 Cycling. SPE/DOE Tenth Symposium on Improved Oil Recovery, April 21–24, Tulsa, OK, US. SPE/DOE 35402
23. Alcorn, Z. P., Fredriksen, S. B., Sharma, M. et al. (2019). An Integrated Carbon-Dioxide-Foam Enhanced-Oil-Recovery Pilot Program With Combined Carbon Capture, Utilization, and Storage in an Onshore Texas Heterogeneous Carbonate Field. SPE Reservoir Evaluation & Engineering-Reservoir Engineering. SPE-190204-PA (in press; posted 27 March 2019). https://doi.org/10.2118/190204-PA.
24. Graue, A., Viksund, B G. and Baldwin, B A. (1999). Reproducible Wettability Alteration of Low-Permeable Outcrop Chalk. *SPE Reservoir Evaluation and Engineering* **2** (02), 134-140. SPE-55904-PA.
25. Steinsbø, M., Brattekås, B., Fernø, M.A., Ersland, G. and Graue, A. (2014). Supercritical CO_2 Injection for Enhanced Oil Recovery in Fracture Chalk. International Symposium of the Society of Core Analysts, 8-12 September, Avignon, France. SCA2014-092.
26. Jian, B., Puerto, M C., Wehowsky, A., Dong, P., Johnston, K P. and Hirasaki, G J. (2016). Static Adsorption of an Ethoxylated Nonionic Surfactant on Carbonate Minerals. *Langmuir* **32** (40), 10244-10252.
27. Steinsbø, M., Brattekås, B., Ersland, G., Bø, K., Opdal, I.E., Tunli, R., Graue, A. and Fernø, M.A. (2015). Foam as Mobility Control for Integrated CO2-EOR in Fractured Carbonates. 18th European Symposium on Improved Oil Recovery, 14-16 April, Dresden, Germany.
28. Hirasaki, G. J. and Lawson, J.B. (1985). Mechanisms of Foam Flow in Porous Media: Apparent Viscosity in Smooth Capillaries. *SPE Journal* **25** (2), 176-190.
29. Johnson, E.F., Bossler, D.P. and Naumann, V.O. (1959). Calculation of Relative Permeability From Displacement Experiments. *Trans. AIME* 1959, *216*, 370-372.
30. Sharma, M., Alcorn Z.P., Fredriksen, S.B., Fernø, M., Graue, A. (2017). Numerical Modeling Study for Designing CO2 Foam Filed Pilot. EAGE IOR Symposium, 24-27 April, Stavanger, Norway.
31. Rognmo, A.U., Fredriksen, S.B., Alcorn, Z.P., Sharma, M., Føyen, T., Eide, Ø., Graue, A. and Fernø, M. (2018). Pore-to-Core EOR Upscaling for CO2-foam for CCUS. SPE EUROPEC featured at the 80th EAGE Annual Conference and Exhibition, 11-14 June, Copenhagen, Denmark. SPE-190869-MS.
32. Eide, Ø., Haugen, Å., Svenningsen, S., Hoff, K., Ersland, G., Fernø, M.A. and Graue, A. (2012). Tertiary Liquid and Supercritical CO_2 injection in Chalk and Limestone at Strongly Water-Wet and Near Neutral-Wet Conditions. International Symposium of the Society of Core Analysts, 27-30 August, Aberdeen, Scotland.
33. Graue, A., Tonheim, E. and Baldwin, B. 1994. Control and Alteration of Wettability in Low-Permeable Chalk". Proceedings of the 3rd International Symposium on Evaluation of Reservoir Wettability and its Effect on Oil Recovery, 21-23 September, Laramie, WY.
34. Eide, Ø., Fernø, M.A., Alcorn, Z.P. and Graue, A. (2016). Visualization of Carbon Dioxide Enhanced Oil Recovery by Diffusion in Fractured Chalk. *SPE Journal* **21** (1), 112-120.
35. Fernø, M A., Steinsbø, M., Eide, Ø., Ahmed, A., Ahmed, K. and Graue, A. (2015). Parametric study of oil recovery during CO_2 injections in fractured chalk: Influence of fracture permeability, diffusion length and water saturation. *Journal of Nat Gas Sci and Eng* **27** (2), 1063-1073.
36. Jadahunandan, P.P. and Morrow, N.R. 1(995). Effect of Wettability on Waterflood Recovery for Crude-Oil/Brine/Rock Systems. *SPE Reservoir Engineering* **10** (1), 40-46.

37. Suffridge, F.E., Raterman, K.T. and Russell, G.C. (1989). Foam Performance Under Reservoir Conditions. 64th SPE ATCE, 8-11 October, San Antonio, Texas, US. SPE-19691-MS.
38. Vikingstad, A. K., Skauge, A., Høiland, H. and Aarra, M. (2005). Foam-oil Interactions Analysed by Static Foam Tests. *Colloids and Surfaces A: Physicochem. Eng. Aspects* **260** (2005), 189-198.
39. T.S. Kristiansen and T. Holt. (1992). Properties of Flowing Foam in Porous Media Containing Oil. Presented at the SPE/DOE Eighth Symposium on Enhanced Oil Recovery, Tulsa, OK, USA, April 22-24, 1992. SPE/DOE 24182.
40. Prud'homme, R K. and Khan, S A. (1996). *Foams, Theory, Measurements, and Applications*. New York: Marcel Dekker Incorporated.

New laboratory core flooding experimental system for EOR surfactant screening, especially for foam

Xuesong Li[1,*], and *Matthias* Appel[1]

[1]Shell Global Solutions International B.V., Special Core Analysis Team, 1031HW Amsterdam, The Netherlands

Abstract. Core flooding experiments are often used to assess the performance of EOR techniques or to screen surfactants. An inherent success factor of chemical EOR processes is the choice of the optimal surfactant which is a trade-off between process performance and economic considerations. Currently, this trade-off can often not fully be evaluated with laboratory experiments because the associated experiments are time consuming which typically limits their number and, in turn, impacts the reliability of the results. For this reason, we aimed to develop an automated and parallel core flooding unit to conduct faster, cheaper and reliable tests for EOR technologies. The benefit of doing this is to dramatically increase the statistics of EOR-related experimentation while decreasing the manpower needed, leading to a much better value-to-cost ratio. As a first step, we designed a setup which is applicable for multiple EOR-related core flooding experiments, such as alkaline-surfactant polymer (ASP), low salinity, polymer flooding or foam injection. The device can be used for co- or sequential injection of gas, water and oil. For the high compressibility gas phase, it is often desirable to regulate its in-core volumetric flow rate. We control the gas flow using inline sensors and flow meters corresponding to the real time in situ core pressure. With a feedback loop, the offset of gas flow can be automatically updated within 0.1% deviation from the target setting. By miniaturizing the core sample and simplifying the experimental procedures, the automated flooding process achieved 90% efficiency gain while reducing sample consumption. This proof of concept can easily be further evolved into a parallelized system. Experience with this new core flooding system demonstrated the dramatic increase in screening capacity and added value to the EOR development workflows.

1 Introduction

There is general consensus about an increasing energy demand in the coming decades. Irrespective of the fact that renewable energy will play an increasing role in the energy supply, the contribution of oil for energy consumption and as feed for chemical production will remain high and is expected to grow. [1]. The current oil market requires a relatively low recovery cost for any field development [2-4] which, in turn, requires faster technology deployment and adequate evaluation of the associated technical risks.

In typical hydrocarbon recovery scenarios, after a primary and secondary recovery, there is still a larger percentage of oil (30-60%) remaining in the reservoir. This remaining oil is primarily trapped by capillary forces [5]. Enhanced oil recovery (EOR) techniques often utilize surfactants to either reduce the interfacial tension between the aqueous phase and oil phase or generate foam to increase the swept efficiency of gas injection [6]. In any of these processes, the selection of the surfactant is essential for the incremental oil recovery. From an economical point of view the cost of surfactant is also a substantial element of the cost of EOR projects [7, 8]. However, the surfactant performance depends on the reservoir fluid and rock properties at field-related temperature and pressure conditions Therefore, it would be ideal to conduct core flooding experiments which combine all these factors for surfactant selections. But when taking all the influencing parameters into account the screening matrix can be very large. For example, Table 1 illustrates the screening program for foam surfactant screening [9]. Even this fairly slimmed down screening program has a matrix size of 100, which would take a few years to complete using a conventional core flooding setup.

Table 1. EOR surfactant screening matrix with reduced variation of variables.

Variables		Variations
1	rock sample type	1
2	rock permeability	1
3	brine salinity	1
4	crude oil	1
5	surfactant type	5
6	surfactant concentration	2
7	rock sample dimension	1
8	flow rate	2
9	temperature	1
10	pressure	1
11	gas/liquid ratio in one test	5
combinations/test numbers		100

* Corresponding author: xuesong.x.li@shell.com